Hover Predictions of S-76 Rotor Using a High-Order Discontinuous Galerkin Off-Body Discretization

Kursat Kara[1],

School of Mechanical and Aerospace Engineering, Oklahoma State University, Stillwater, OK 74078

Andrew C. Kirby[2], and Dimitri J. Mavriplis[3]

Department of Mechanical Engineering, University of Wyoming, Laramie, WY 82071

Hover performance of a four-bladed Sikorsky S-76 rotor is studied using a high-order discontinuous Galerkin (DG) off-body discretization. Time accurate Navier-Stokes calculations are performed using the W^2A^2KE3D code, which combines solution technologies in a multi-mesh, multi-solver paradigm through a dynamic overset framework that employs an unstructured mesh Navier-Stokes method as a near-body solver and a high-order adaptive discontinuous Galerkin discretization as an off-body solver. The rotor with a swept-tapered tip is simulated. The tip Mach number was 0.65, and the Reynolds number based on the reference chord is 1.2 million. A constant coning angle of 3.5° is applied. The effect of time step size and sub-iterations on the integrated parameters is investigated and convergence results are presented. The effect of the maximum order of accuracy of the adaptive h-p discretization in the off-body solver on solution accuracy and efficiency is also investigated. Thrust coefficient, torque coefficient and figure of merit are calculated and compared with available data in the literature, and good agreement is found. In general, higher order off-body simulations are found to result in a better accuracy/cost metric.

Nomenclature

a_∞	=	freestream speed of sound, ft/s
c	=	local chord, in.
c_e	=	equivalent chord, in.
c_{ref}	=	reference chord, in.
C_Q	=	rotor torque coefficient, $\frac{Q}{\left(\frac{1}{2}\pi\rho\Omega^2 R^5\right)}$
C_T	=	rotor thrust coefficient, $\frac{T}{\left(\frac{1}{2}\pi\rho\Omega^2 R^4\right)}$
FM	=	figure of merit, $\frac{C_T^{3/2}}{(\sqrt{2}C_Q)}$
M_{tip}	=	tip Mach number, $\frac{\Omega R}{a_\infty}$
N_b	=	number of blades
Q	=	rotor torque, ft · lbf
R	=	blade radius, in.
Re_{cref}	=	Reynolds number based on c_{ref}
r	=	rotor radial axis
T	=	rotor thrust, lbf

---

[1] Assistant Professor, AIAA Senior Member
[2] Postdoctoral Researcher, AIAA Member
[3] Professor, AIAA Associate Fellow

z	=	rotor axial axis
θ	=	blade section twist, deg
θ_c	=	collective pitch, deg
ρ	=	density, $slug/ft^3$
σ	=	rotor solidity, $\frac{N_b c_{ref}}{\pi R}$
Ω	=	rotor rotational speed, rad/s
ω	=	vorticity magnitude

I. Introduction

An accurate prediction of hover performance is a critical design objective for helicopter operation, and it is a limiting design point in terms of power requirements. The Rotorcraft Working Group of the AIAA Applied Aerodynamics Technical Committee was established to assess the state of the art and guide the future directions of hover prediction technology[1–3]. In the first Rotorcraft Hover Prediction Workshop, a brief review[1] of the historical progress of hover predictions and wake capturing was presented. The focus of the review was on the Navier-Stokes based "first-principles" wake capturing, high-order methods, overset grid, and adaptive mesh refinement (AMR). The working group identified a publicly available four-bladed S-76 rotor[4] for the standardized evaluations. For the first workshop, Sikorsky and Georgia Tech together produced an accurate representation of the S-76 scaled rotor surface geometry. A refined surface grid with 291 axial and 98 radial grid points was generated and provided to all the participants by the Rotor Simulation Working Group[1].

During the last five years, several Navier-Stokes based simulations showed good agreement on integrated performance numbers such as thrust and torque coefficients and figure of merit. Initial efforts of the workshop focused on the prediction of S-76 performance for a single blade-tip[5–8]. Later, the S-76 rotor was investigated for three different blade tip-shapes, e.g., rectangular tip, swept-tapered tip, and swept-tapered-anhedral tip[9–11]. Simulations were performed for tip Mach numbers of 0.55, 0.60, and 0.65 and collective pitch angles of 6-10 deg. Reported results showed a good agreement with integrated performance parameters such as thrust coefficient, torque coefficient, and figure of merit (FM). However, radial pressure distributions differed significantly.

For industrial applications, the rotor FM is used as an efficiency metric, and it may be a decision-maker between competing designs. Therefore, an accurate prediction of the FM is critically essential for a new rotor blade design. Ref. [3] discussed a list of issues that might affect the FM, such as grid independency, temporal accuracy, solution convergence, wake breakdown, installation effects, aeroelastic effects, transition modeling. Moreover, Ref. [3] provided a list of potential topics. The goal of this paper is to investigate the accuracy and efficiency of an overset unstructured mesh near-body and high-order accurate adaptive off-body discretization for predicting rotor hover performance metrics as well as for resolving important wake features.

II. Numerical Methodology

W^2A^2KE3D is a computational methodology that combines solution technologies in a multi-mesh, multi-solver paradigm through a dynamic overset framework[12,13]. The mesh system generally consists of a collection of unstructured *near-body* and Cartesian *off-body* meshes. The two computational fluid dynamics (CFD) solvers are linked by a Topology Independent Overset Grid Assembler (TIOGA)[14,15], which dynamically interpolates the solution between the meshes. A detailed description of the W^2A^2KE3D computational framework is provided in reference[12].

NSU3D[16,17] is used as the near-body solver. The NSU3D code is an unstructured mesh, multigrid, Reynolds averaged Navier–Stokes solver for high-Reynolds-number external aerodynamic applications. The NSU3D discretization employs a vertex-based approach, where the unknown fluid and turbulence variables are stored at the vertices of the mesh and fluxes are computed on faces delimiting dual control volumes, with each dual face being associated with a mesh edge[17]. This discretization operates on hybrid mixed-element meshes, generally employing prismatic elements in highly stretched boundary-layer regions and tetrahedral elements in isotropic regions of the mesh away from the aircraft surfaces. A single edge-based data structure is used to compute flux balances across all types of elements. The convective terms are discretized as central differences with added matrix dissipation. Second-order accuracy is achieved by formulating these dissipative terms as an undivided biharmonic operator, which is constructed in two passes of a nearest-neighbor Laplacian operator. The solver uses automatic agglomeration

multigrid along with line-implicit preconditioning for accelerated solution convergence. Additionally, NSU3D has served as a near-body flow solver in the CREATE-AV HELIOS[18,19] software.

The off-body solver is CartDG[12,20], which is a high-order, Cartesian, discontinuous Galerkin (DG), adaptive mesh refinement (AMR) solver. It uses an Octree-based AMR library called p4est[21] which provides h-adaptation. In addition, it incorporates a p-refinement capability which allows each cell to have a variable polynomial degree[14,20]. CartDG employs a p-adaption strategy for the off-body solver that favors low polynomial degrees and fine meshes where the off-body is in close proximity to the near-body, and high polynomial degrees away from the near-body. The p-adaption strategy for the off-body solver can be summarized with these four rules[20]:

- Refine and match the off-body resolution both in mesh size and accuracy with that of the near-body mesh in close proximity to the overlap region of the overset grids.
- Increase the polynomial degree in the off-body region as quickly as possible without creating a more restrictive time step by simultaneously increasing the mesh size and raising the polynomial degree of the discretization.
- Refine the mesh to flow features using the highest possible polynomial degree.
- Refine elements to stay ahead of propagating flow features. This is implemented by refining any neighboring cells that share a face with a cell that has been tagged for flow feature refinement.

To detect a flow feature, the solution gradients are used, and the Q criterion is calculated at the quadrature points of the high-order discretization in each mesh cell. If the Q criterion at a quadrature point is greater than a tolerance τ, then the cell is tagged for refinement.

CartDG discretizes the compressible Navier–Stokes equations. Details of the algorithm are outlined in reference[22] and several performance statistics for a wide range of orders of solution accuracy are provided in the literature[12,13,22]. To maximize performance, CartDG is designed using a tensor-product, collocation-based DG method making simplifications for Cartesian meshes when available. Through this approach, the numerical complexity is reduced and very high computational rates can be achieved. Perhaps more importantly, the cost of a residual evaluation per degree of freedom actually decreases as the order p of the discretization is increased. This is depicted in Figure 1, where the cost of a residual evaluation per degree of freedom for the CartDG explicit solver is plotted as a function of the order p of the discretization for both the traditional finite-element formulation and for the tensor-product formulation. As seen in the figure, the cost per degree of freedom decreases initially from p=1 to p=8 (ninth order) and remains approximately constant for higher p orders. Because higher-order accurate discretizations generally deliver superior accuracy than lower order accurate methods using equivalent numbers of degrees of freedom (for smooth solutions), the trends shown in Figure 1 suggest that the use of very high order (i.e. up to p=10) discretizations in wake regions can be beneficial both in terms of accuracy and computational efficiency.
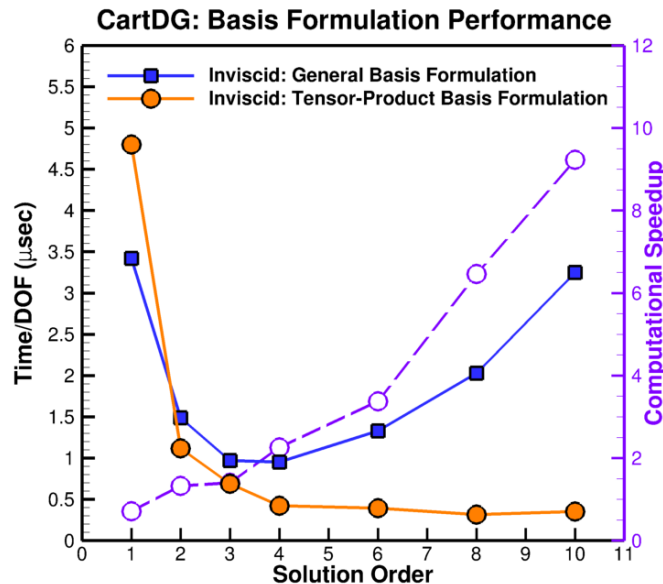

Figure 1: Comparison of time per degree of freedom for general formulation versus tensor-product formulation for CartDG off-body solver up to p=10 order of accuracy

3

III. Problem Description

The S-76 blade with a swept-tapered tip is studied using the W^2A^2KE3D computational framework. The objective of this work is to investigate the use of high-order discretizations on the accuracy and efficiency of rotorcraft problems in general, starting with hover problems in particular in this paper. At the same time, the effect of other parameters such as time step size and algebraic convergence levels for the near-body solver are studied prior to the investigation of p-order discretizations in the off-body regions in order to assess the relative effect of these different error sources. The S-76 rotor hover experiments[4] were performed at the Sikorsky Model Hover Test Facility using the basic model test rig. Performance parameters were measured on the 1:4.71 model-scale rotor for a number of rotor configurations and conditions. The experiments considered the S-76 rotor with five different tips (rectangular, swept, tapered, swept-tapered, and swept-tapered-anhedral), three different blade tip Mach numbers, in-ground effect, and out-of-ground effect test conditions. The S-76 rotor blade airfoil, chord, and sweep distributions are shown in Fig. 2. The rotor radius is 56.04 in. and the reference chord length is 3.1 in. The rotor uses airfoils SC1013R8, SC1095R8, SC1095[4]. The rotor has four blades with a solidity of 0.07043.

In the present work, the rotor is assumed to be rigid, an isolated rotor hovering out-of-ground at standard day sea-level conditions. The collective pitch angle is applied by pitching the whole blade. A constant coning angle of 3.5° is applied to all blades. The collective pitch angle is varied from 4 to 12 degrees in the simulations. Blade flapping motion and facility effects are not considered in this study. The swept-tapered tip shape is simulated at a tip Mach number of 0.65 and the Reynolds number based on the reference chord is 1.2 million.

Table 1 shows the list of simulations parameters used in the present study. In order to investigate the efficiency and accuracy of high-order accurate discretizations, simulations were performed with maximum orders of $p_{max}=3$, 5 and 7 in the off-body regions. As mentioned in the previous section, the W^2A^2KE3D solver employs a dual-mesh approach where near-body meshes are used for the rotor blades and the generic hub, and an off-body Cartesian mesh is automatically created to enclose the near-body meshed as shown in Fig. 3. For the near body solver each blade was fitted with an unstructured strand mesh containing a total of 4,542,723 mesh points per blade with suitable near-wall resolution and the hub was discretized using an unstructured mesh of 289,410 points. The employed near-body meshes are the same meshes used previously in references[23,24]. The off-body mesh consists of a simple Cartesian mesh which is adaptively refined as the simulation progresses. The outer boundaries of the off-body mesh are located at 10R from the rotor center. Figure 4 shows all four blades, the hub, near-body, and surrounding off-body meshes.
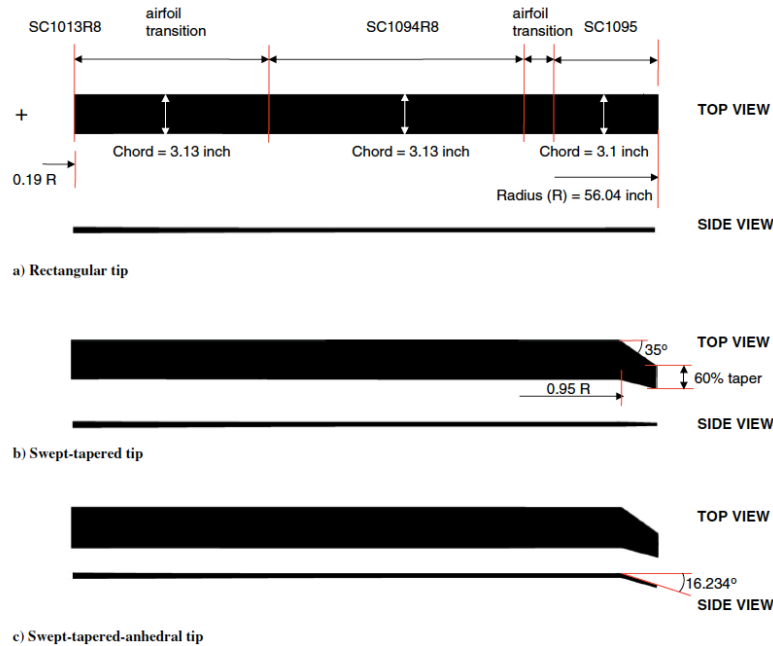

Figure 2. Sikorsky S-76 rotor blade airfoil, chord, and swept distributions for different tip shapes (Ref. [23]).

Table 1. List of simulation parameters.

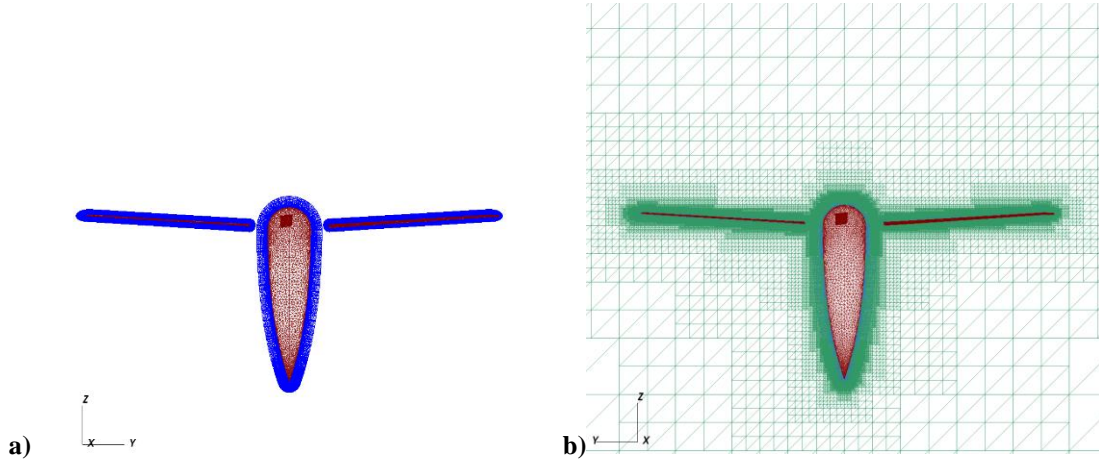| Tip Shape	M_{tip}	Re_c (10^6)	θ_c (degrees)	p_{max}
Swept-tapered	0.65	1.2	4, 6, 8, 10, 12	3, 5, 7

Figure 3. a) Near-body meshes of the S-76 rotor blades and generic hub b) off-body mesh in the YZ plane.
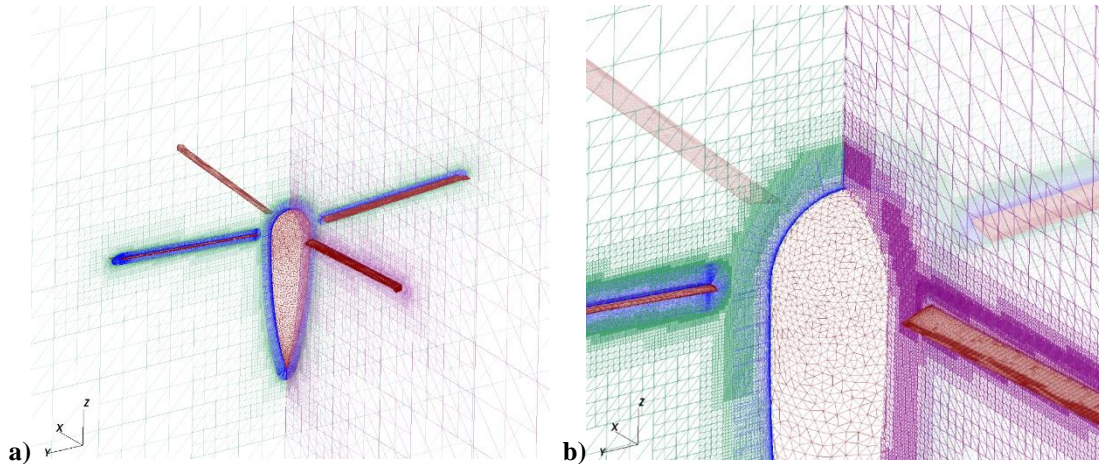

Figure 4. Near-body and off-body meshes of S-76 rotor and hub.

IV. Results: Time Step Size and Algebraic Convergence Effects

A set of initial simulations were performed to study the effect of the time step size and convergence of the implicit system at each time step of the near-body solver on the overall rotor aerodynamic performance coefficients. The near-body solver employs an implicit BDF2 time discretization which is solved using a line-implicit multigrid strategy. The off-body solver is explicit in time, and performs the required number of explicit time steps to synchronize with the each implicit time step of the near-body solver. For the time step study, the number of sub-iterations in the near-body solver (NSU3D) was fixed at 25 multigrid cycles, and computations were run for a minimum of 0.5 rotor revolutions. Although longer time simulations are desirable, focusing the time step study on the start-up transient region provides a realistic test of temporal accuracy since this is the region with the most rapid temporal variations. Simulations using time steps corresponding to 1/2°, 1/4° and 1/10° rotor rotation were

performed. For these cases the tip Mach number was 0.65, and the collective pitch angle was 10°. Figure 5 depicts the computed thrust coefficient C_T, showing only very small differences between the various time step runs. Details of the time histories are shown in Figure 5(b), where the differences in this region are seen to be less than 0.1% between the two smallest time steps, and the values appear to be converging with decreasing time step size.

In Figure 6, the convergence of the near-body implicit solver is examined. The convergence of the implicit system, as monitored by the decrease in the residual of the density equation, is shown using 25 multigrid iterations for the three time step sizes of 1/2°, 1/4° and 1/10° rotation. As expected, faster convergence rates are observed for smaller time step sizes. Using a time step of 1/2° rotation, the density residual is decreased by approximately 2.5 orders of magnitude in 25 multigrid cycles, whereas a 4.5 order of magnitude decrease in the residual is achieved using the smallest time step of 1/10°. In Figure 6(b), the convergence level at a fixed time step of 1/2° is studied. Here, the convergence is seen to be monotone and relatively constant, achieving approximately 3 orders of magnitude reduction with 25 multigrid cycles, and close to 9 orders of magnitude reduction using 100 multigrid cycles.

Little difference in the overall computed performance coefficients of the rotor could be found using between 25 and 100 multigrid cycles per time step, over the first revolution. Based on these results, and previous results for wind turbine configurations[12], a time step size of 1/4° using 40 multigrid sub-iterations was chosen for all subsequent long time history computations. Using these parameters, the cost of a simulation for one rotor revolution requires approximately 24 hours on 5,400 cores of the NCAR-Wyoming Cheyenne supercomputer, although this number can vary significantly depending on the amount of wake refinement which occurs adaptively.

V. Results: P-Order Discretization Effects

The effects of the polynomial degree of spatial accuracy in the off-body mesh elements on the integrated parameters are studied in this section. The off-body solver allows for h-adaption (mesh refinement) and p-enrichment (variable polynomial degree of solution approximation within a mesh element). In general, the expectation is that the use of higher-order accurate discretizations in wake regions should lead to more efficient and accurate simulation results based on the timings discussed in Figure 1 in Section II. A set of simulations run with varying values of maximum polynomial degrees from 3 to 7 and integrated performance parameters such as thrust, torque and the figure of merit are calculated over several revolutions. The hp-adaption strategy permits the minimum polynomial degree to persist on the finest mesh level in the near-body/off-body mesh overlap regions. The strategy then grows the polynomial degrees as the mesh elements coarsen to the maximum allowable polynomial degree. The simulations herein have a collective pitch angle of 10° and the time step is set to 1/4° rotation. The near-body solver, NSU3D, uses 40 sub-iterations to converge the multi-grid algorithm with four mesh levels. After two revolutions, the performance parameters converge to near constant values, and close inspection reveals an oscillatory behavior around a mean value as shown in Figure 7. Increasing the maximum polynomial degree in the off-body mesh elements from 3 to 7 is seen to have very little effect on the integrated performance parameters such as thrust, torque and the figure of merit as shown in Figure 7.

Figures 8 and 9 show the off-body mesh and iso-surface of velocity magnitude. In this case, the off-body grid is adapted using $p_{max}=3$, and spatial resolution around the tip-vortex is visible. Turning now to higher p_{max} simulations, the iso-surface of velocity magnitude is shown in Fig. 10 for the maximum polynomial degree of seven ($p_{max}=7$), which provides eighth-order accuracy. A well-defined helical blade tip-vortex structure and a stronger circular vortex from the first revolution are visible. The wake contracts axially downward from the rotor plane and the first tip-vortex starts to roll-up and expand axially as shown in Fig. 11. Although the helical vortex structure is clearly visible at the fifth revolution as shown in Fig. 11a, the vortex structure disintegrates in the following revolutions as depicted in Fig. 11b. Mesh plots in Fig. 11c-d shows that AMR is capturing the helical vortex structure and dissipated parts. Note that in Figure 8, 9 and 11, the mesh is rendered with subgrid structures in each finite-element or Cartesian cell, in order to capture the full resolution of the high order discretizations.

The variation of the total number of degrees of freedom (DOFs) for the off-body mesh with advancing time is shown in Fig. 12 and the DOF counts are presented in Tables 2-4. For $p_{max}=5$, the simulation shown in Fig. 12b, at the initial stage (1/4 revolution), the total number of DOFs is approximately 160 million. This increases to 520 million at the end of four revolutions. In this simulation, p=2 and p=3 elements are used in overlap regions to connect the near-body and off-body meshes, and the $p_{max}=5$ value is used further away in wake regions. Therefore, the average number of DOFs remain relatively constant for p=2 and p=3, and the small variations are due to near-body mesh alignment with the principle axes of Cartesian off-body mesh as shown in Fig. 12b. However, the number of $p_{max}=5$ cells grows as the wake is convected downstream. Similar behavior is also displayed for the

p_{max}=7 simulation shown in Fig. 12c with the number of p=2, 3, and 5 elements remaining relatively constant, and the number of p_{max}=7 elements growing in time. Table 5 compares the timings of different off-body p-orders. According to the data, the p_{max}=5 (6th order accurate) off-body simulation takes 10.1 seconds at the 360th time-step where the tip-vortex is developing in the rotor plane. The computation time is 9.6 and 11.4 seconds for p_{max} of 3 and 7, respectively. At the end of the 4th revolution, the total number of DOFs of p_{max}=5 increases to 520 million and the computation time doubles to 20.5 seconds. On the other hand, the p_{max}=7 simulation takes only 11.99 seconds with 298 million elements, as shown in Tables 4 and 5. Results show that p_{max}=7 (8th order accurate) simulation estimates the integrated performance parameters accurately by employing 42.6% fewer DOFs than the p_{max}=5 (6th order accurate) simulation.

Table 2. The degree of freedom counts for the off-body mesh adaptation of p_{max} = 3.

N	P2 DOFs	P3 DOFs	Total DOFs
360 (1/4th Rev.)	68,433,984	78,099,520	146,533,504
5440 (4th Rev.)	53,025,408	358,521,920	411,547,328

Table 3. The degree of freedom counts for the off-body mesh adaptation of p_{max} = 5.

N	P2 DOFs	P3 DOFs	P5 DOFs	Total DOFs
360 (1/4th Rev.)	69,178,968	32,431,552	57,417,768	159,028,288
5440 (4th Rev.)	54,413,640	25,972,032	439,234,048	519,619,712

Table 4. The degree of freedom counts for the off-body mesh adaptation of p_{max} = 7.

N	P2 DOFs	P3 DOFs	P5 DOFs	P7 DOFs	Total DOFs
360 (1/4th Rev.)	69,211,152	32,412,800	28,527,768	35,290,624	165,442,336
5440 (4th Rev.)	54,032,400	26,075,264	24,336,072	193,454,080	297,897,824

Table 5. The timings of off-body mesh adaptation orders

CartDG	time (N = 360)	time (N = 5440.)	time/Total DOFs (N = 360)	time/Total DOFs (N = 5440)
p_{max} = 3	9.63612	18.95282	6.576E-08	4.605E-08
p_{max} = 5	10.99994	20.50581	6.917E-08	3.946E-08
p_{max} = 7	11.43535	11.98945	6.912E-08	4.025E-08

VI.   Collective Sweep Results

The ability of the W^2A^2KE3D framework to make quantitative calculations of the integrated performance metrics of the S-76 rotor in hover is studied in this section. As previously, the tip Mach number of 0.65 and the Reynolds number based on the reference chord is 1.2 million. Fully turbulent flow is assumed, and the Spalart-Allmaras based DES model is used in the near-body solver, while a simple constant Smagorinsky sub-grid scale model is used in the off-body solver. The time step size is taken as 1/4° rotation and 40 multigrid cycles are used in the near-body solver at each implicit time step. A collective pitch angle sweep is performed by running simulations for collective pitch angles of 4, 6, 8, 10, and 12 degrees. The results in terms of computed thrust, power and figure of merit are shown in Figure 13 where they are compared with experimental values[4] and computational results previously obtained using the HELIOS software[23]. Overall, the results are in good agreement with both experimental values and the values produced by HELIOS, which used the same near-body meshes, although slight variations exist at 6- and 10-degree collective pitch angles.

VII. Conclusions

In this paper the use of a hybrid near-body/off-body overlapping mesh solver approach for rotorcraft simulations is investigated for simulation of the S76 rotor in hover. The particular approach employs a high-order discontinuous Galerkin discretization in the off-body region, which employs both h and p refinement. Based on timings of the standalone DG solver which shows high order discretization to be more efficient than lower order discretizations, the expectation is that using very high order discretizations in wake regions may enable more accurate and efficient rotorcraft simulations. The results show that simulations using up to 8th order accuracy in wake regions produce equivalent results employing lower numbers of degrees of freedom and requiring less computational resources. However, a precise accuracy study is still lacking due to the difficulty in formulating rigorous accuracy metrics. Additionally, increased wake resolution was shown to have only a small effect on overall integrated rotor performance metrics such as thrust coefficient and figure of merit. Finally, the present approach show good agreement with experimental results and previously published computational results for the S76 rotor. Future work will focus on devising suitable error estimation criteria which can be used to drive the h-p refinement strategy developed in this work in a more optimal manner.

Acknowledgments

References

1. Hariharan N, Egolf A, Sankar L. Simulation of Rotor in Hover: Current State, Challenges and Standardized Evaluation. In: *52nd Aerospace Sciences Meeting*. Reston, Virginia: American Institute of Aeronautics and Astronautics; 2014. doi:10.2514/6.2014-0041
2. Hariharan N, Egolf A, Narducci R, Sankar L. Helicopter Rotor Aerodynamic Modeling in Hover: AIAA Standardized Hover Evaluations. In: *53rd AIAA Aerospace Sciences Meeting*. Reston, Virginia: American Institute of Aeronautics and Astronautics; 2015. doi:10.2514/6.2015-1242
3. Hariharan N, Narducci R, Reed E, Egolf A. AIAA Standardized Hover Simulation: Hover Performance Prediction Status and Outstanding Issues. In: *55th AIAA Aerospace Sciences Meeting*. Reston, Virginia: American Institute of Aeronautics and Astronautics; 2017:1-17. doi:10.2514/6.2017-1429
4. Balch DT, Lombardi J. *NASA CR 177336 Experimental Study of Main Rotor Tip Geometry and Tail Rotor Interactions in Hover. Vol I - Text and Figures.*; 1985. https://archive.org/details/NASA_NTRS_Archive_19850014034/page/n14.
5. Jain R, Potsdam MA. Hover Predictions on the Sikorsky S-76 Rotor using Helios. In: *52nd Aerospace Sciences Meeting*. Reston, Virginia: American Institute of Aeronautics and Astronautics; 2014:1-22. doi:10.2514/6.2014-0207
6. Sheng C, Zhao Q, Wang J. S-76 Rotor Hover Prediction Using U2NCLE Solver. In: *52nd Aerospace Sciences Meeting*. Reston, Virginia: American Institute of Aeronautics and Astronautics; 2014:1-20. doi:10.2514/6.2014-0044
7. Tadghighi H. Helios Simulation of Rotors in Hover: The Boeing Company. In: *52nd Aerospace Sciences Meeting*. Reston, Virginia: American Institute of Aeronautics and Astronautics; 2014:1-10. doi:10.2514/6.2014-0209
8. Narducci R. OVERFLOW Simulation of Rotors in Hover: The Boeing Company. In: *52nd Aerospace Sciences Meeting*. Reston, Virginia: American Institute of Aeronautics and Astronautics; 2014:1-10. doi:10.2514/6.2014-0208
9. Jain R. Hover Predictions for the S-76 Rotor with Tip Shape Variation using CREATE-AV Helios. In: *53rd AIAA Aerospace Sciences Meeting*. Reston, Virginia: American Institute of Aeronautics and Astronautics; 2015:1-29. doi:10.2514/6.2015-1244
10. Hwang JY, Choi JH, Kwon OJ. Assessment of S-76 Rotor Aerodynamic Performance in Hover on Unstructured Mixed Meshes. In: *53rd AIAA Aerospace Sciences Meeting*. Reston, Virginia: American Institute of Aeronautics and Astronautics; 2015:1-19. doi:10.2514/6.2015-1246
11. Sankar L, Marpu R, Hariharan N, Egolf A. Assessment of Planform Effects on Rotor Hover Performance. In: *53rd AIAA Aerospace Sciences Meeting*. Reston, Virginia: American Institute of Aeronautics and Astronautics; 2015:1-12. doi:10.2514/6.2015-1716
12. Kirby AC, Brazell MJ, Yang Z, et al. Wind farm simulations using an overset hp -adaptive approach with blade-resolved turbine models. *Int J High Perform Comput Appl*. March 2019:1-27. doi:10.1177/1094342019832960
13. Kirby AC, Hassanzadeh A, Mavriplis DJ, Naughton JW. Wind Turbine Wake Dynamics Analysis Using a High-Fidelity Simulation Framework with Blade-Resolved Turbine Models. In: *2018 Wind Energy Symposium*. Reston, Virginia: American Institute of Aeronautics and Astronautics; 2018:1-22. doi:10.2514/6.2018-0256

14. Brazell MJ, Sitaraman J, Mavriplis DJ. An overset mesh approach for 3D mixed element high-order discretizations. *J Comput Phys*. 2016;322:33-51. doi:10.1016/j.jcp.2016.06.031

15. Roget B, Sitaraman J. Robust and efficient overset grid assembly for partitioned unstructured meshes. *J Comput Phys*. 2014;260:1-24. doi:10.1016/j.jcp.2013.12.021

16. Mavriplis D. Grid Resolution Study of a Drag Prediction Workshop Configuration Using the NSU3D Unstructured Mesh Solver. In: *23rd AIAA Applied Aerodynamics Conference*. Reston, Virigina: American Institute of Aeronautics and Astronautics; 2005:1-16. doi:10.2514/6.2005-4729

17. Mavriplis D, Long M. NSU3D Results for the Fourth AIAA Drag Prediction Workshop. *J Aircr*. 2014;51(4):1161-1171. doi:10.2514/1.C032556

18. Wissink AM, Potsdam M, Sankaran V, Sitaraman J, Mavriplis D. A Dual-Mesh Unstructured Adaptive Cartesian Computational Fluid Dynamics Approach for Hover Prediction. *J Am Helicopter Soc*. 2016;61(1):1-19. doi:10.4050/JAHS.61.012004

19. Abras J, Hariharan N. Comparison of CFD Hover Predictions on the S-76 Rotor. In: *53rd AIAA Aerospace Sciences Meeting*. Reston, Virginia: American Institute of Aeronautics and Astronautics; 2015:1-12. doi:10.2514/6.2015-1711

20. Brazell MJ, Kirby AC, Mavriplis D. A high-order discontinuous-Galerkin octree-based AMR solver for overset simulations. In: *23rd AIAA Computational Fluid Dynamics Conference*. Reston, Virginia: American Institute of Aeronautics and Astronautics; 2017:1-28. doi:10.2514/6.2017-3944

21. Burstedde C, Wilcox LC, Ghattas O. p4est : Scalable Algorithms for Parallel Adaptive Mesh Refinement on Forests of Octrees. *SIAM J Sci Comput*. 2011;33(3):1103-1133. doi:10.1137/100791634

22. Kirby AC, Mavriplis DJ, Wissink AM. An Adaptive Explicit 3D Discontinuous Galerkin Solver for Unsteady Problems. In: *22nd AIAA Computational Fluid Dynamics Conference*. Reston, Virginia: American Institute of Aeronautics and Astronautics; 2015:1-23. doi:10.2514/6.2015-3046

23. Jain R. Hover Predictions on the S-76 Rotor with Tip Shape Variation Using Helios. *J Aircr*. 2018;55(1):66-77. doi:10.2514/1.C034075

24. Jain R. Sensitivity Study of High-Fidelity Hover Predictions on the Sikorsky S-76 Rotor. *J Aircr*. 2018;55(1):78-88. doi:10.2514/1.C034076
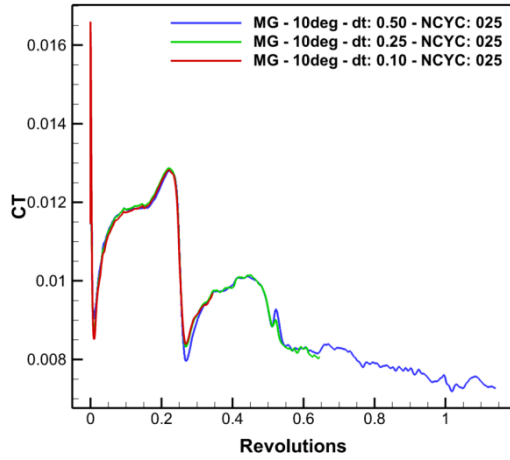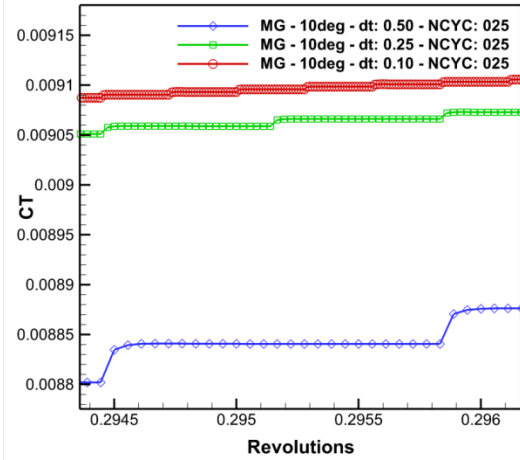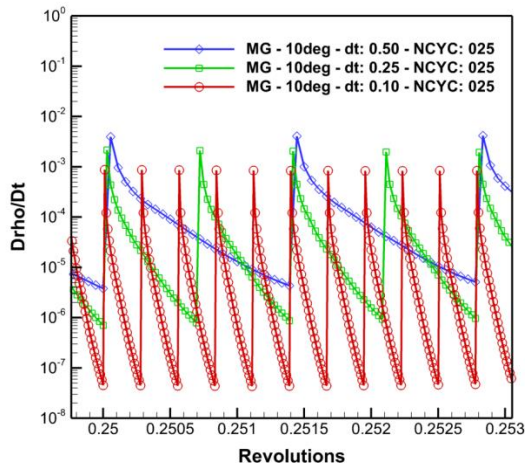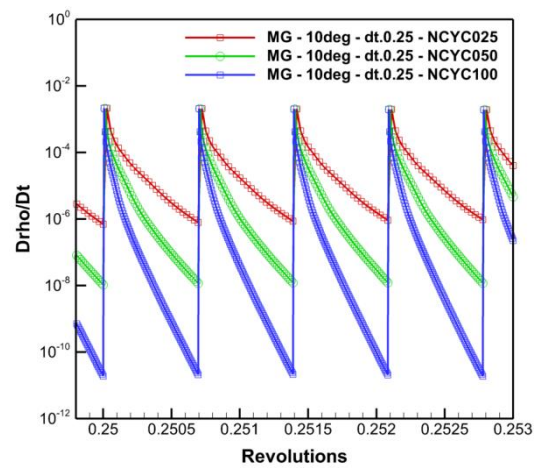
Figure 5. Thrust coefficient of S-76 rotor at a collective pitch angle of 10°. Each simulation uses a time step corresponding to 1/2°, 1/4° and 1/10° rotation. Near-body solver NSU3D is using 25 sub-iterations.

Figure 6. Comparison of density residual of S-76 rotor at collective pitch angle of 10°. a) Effect of the time step. Each simulation uses a time step corresponding to 1/2°, 1/4° and 1/10° rotation. b) Effect of the number of sub-iterations on density residual using a time step corresponding to 1/2° rotor rotation.

(a)

(b)

(c)
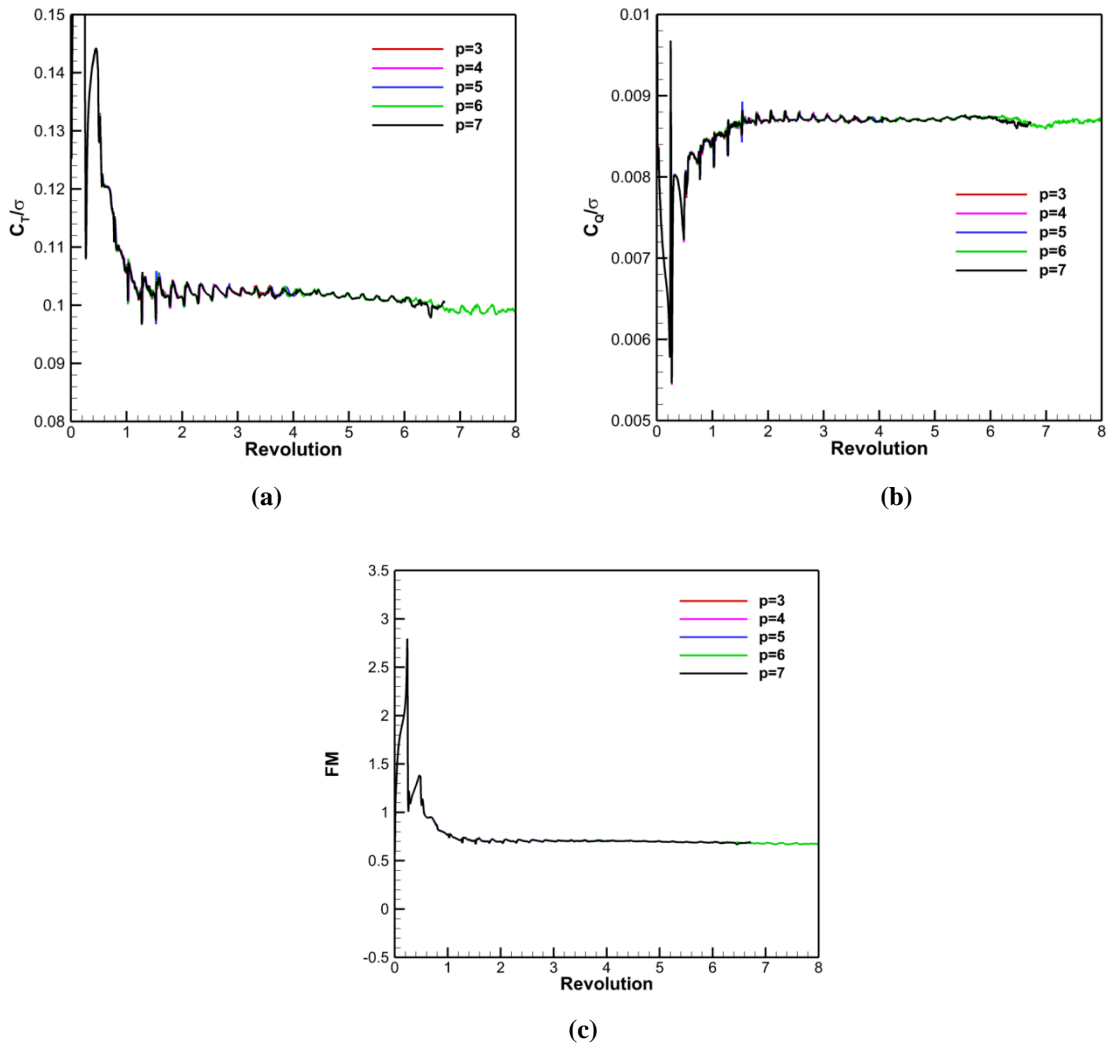
Figure 7. Time history of the S-76 rotor performance parameters. a) thrust coefficient, b) torque coefficient, and c) the figure of merit. The number of sub-iterations is 40 for the near-body flow solver, NSU3D. The collective pitch angle is 10° and the time step is 1/4° rotation.
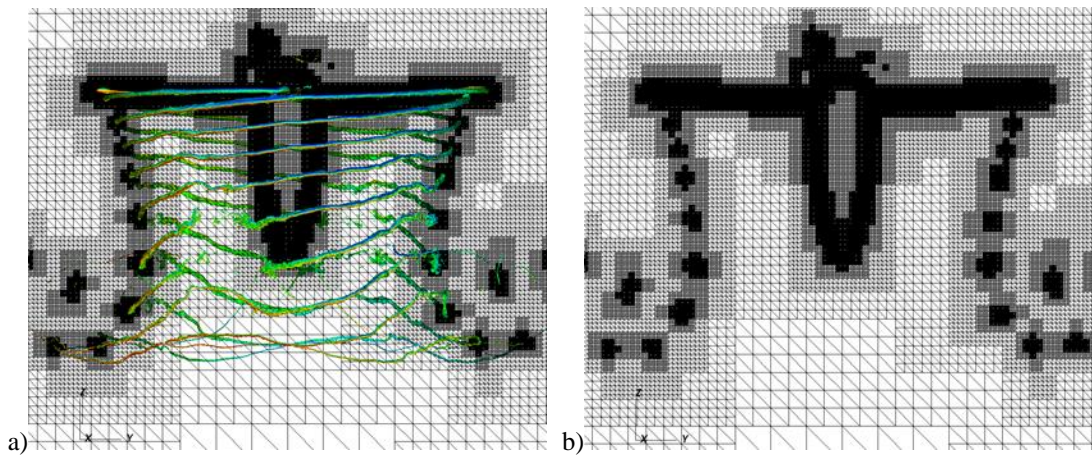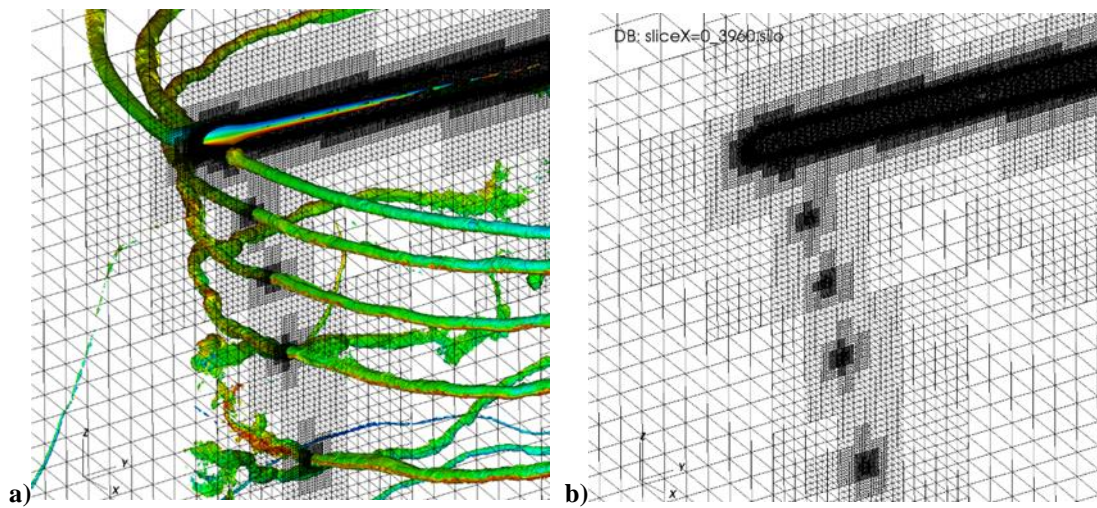
Figure 8. WAKE3D results for S-76 rotor with the swept-tapered tip at Mtip=0.65 in the YZ plane using p_{max}=3. a) Iso-surface of velocity magnitude showing the wake b) off-body mesh showing adapted mesh.

Figure 9. WAKE3D results for the S-76 rotor with the swept-tapered tip at Mtip=0.65 using p_{max}=3 a) Iso-surface of velocity magnitude b) off-body mesh showing AMR capability.
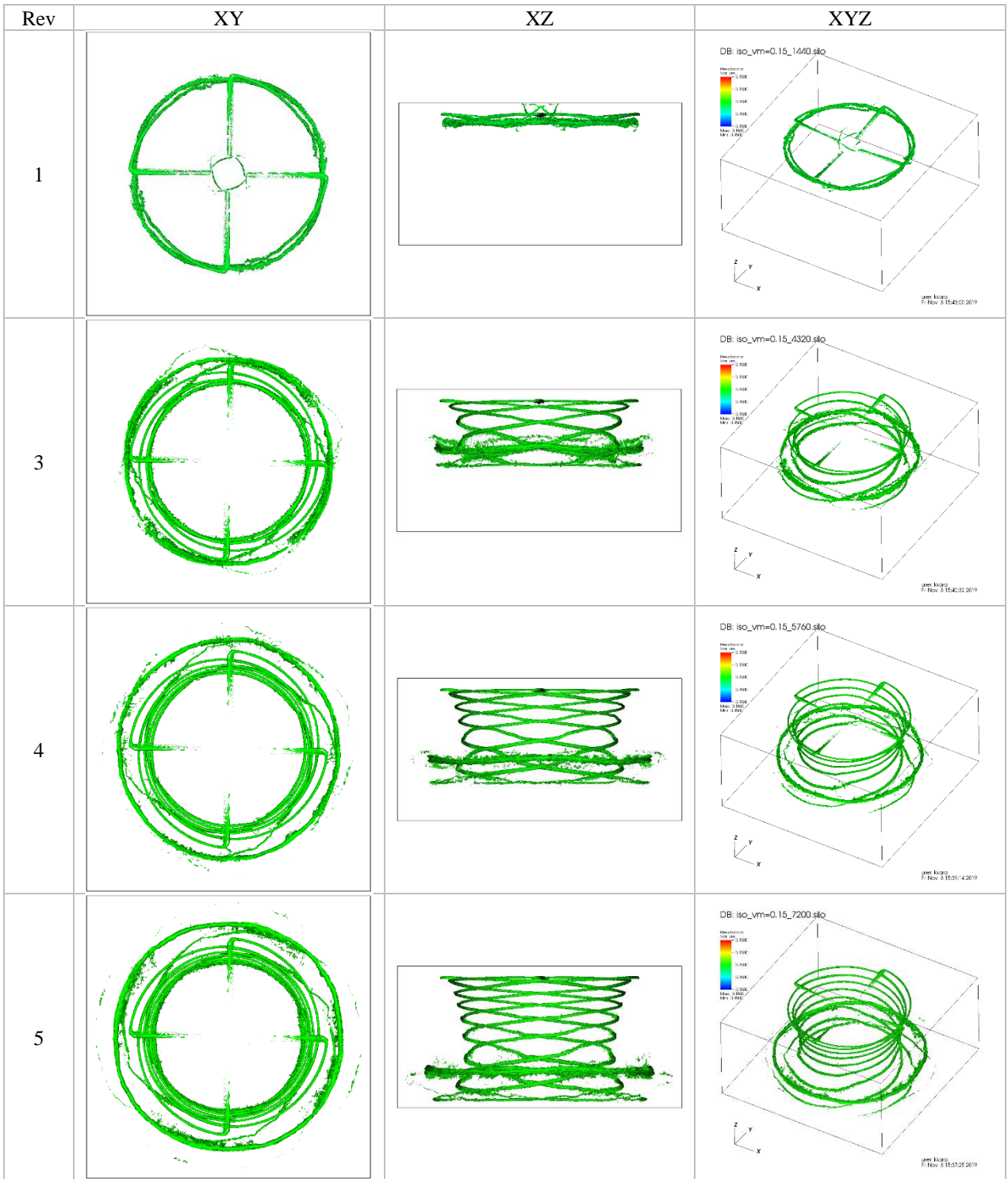
Figure 10. Wake history of the S-76 rotor with the swept-tapered tip at M_{tip}=0.65. The simulation uses p_{max} of 7. Iso-surface of velocity magnitude=0.15 is plotted. Columns show the viewing planes and rows show the revolution.
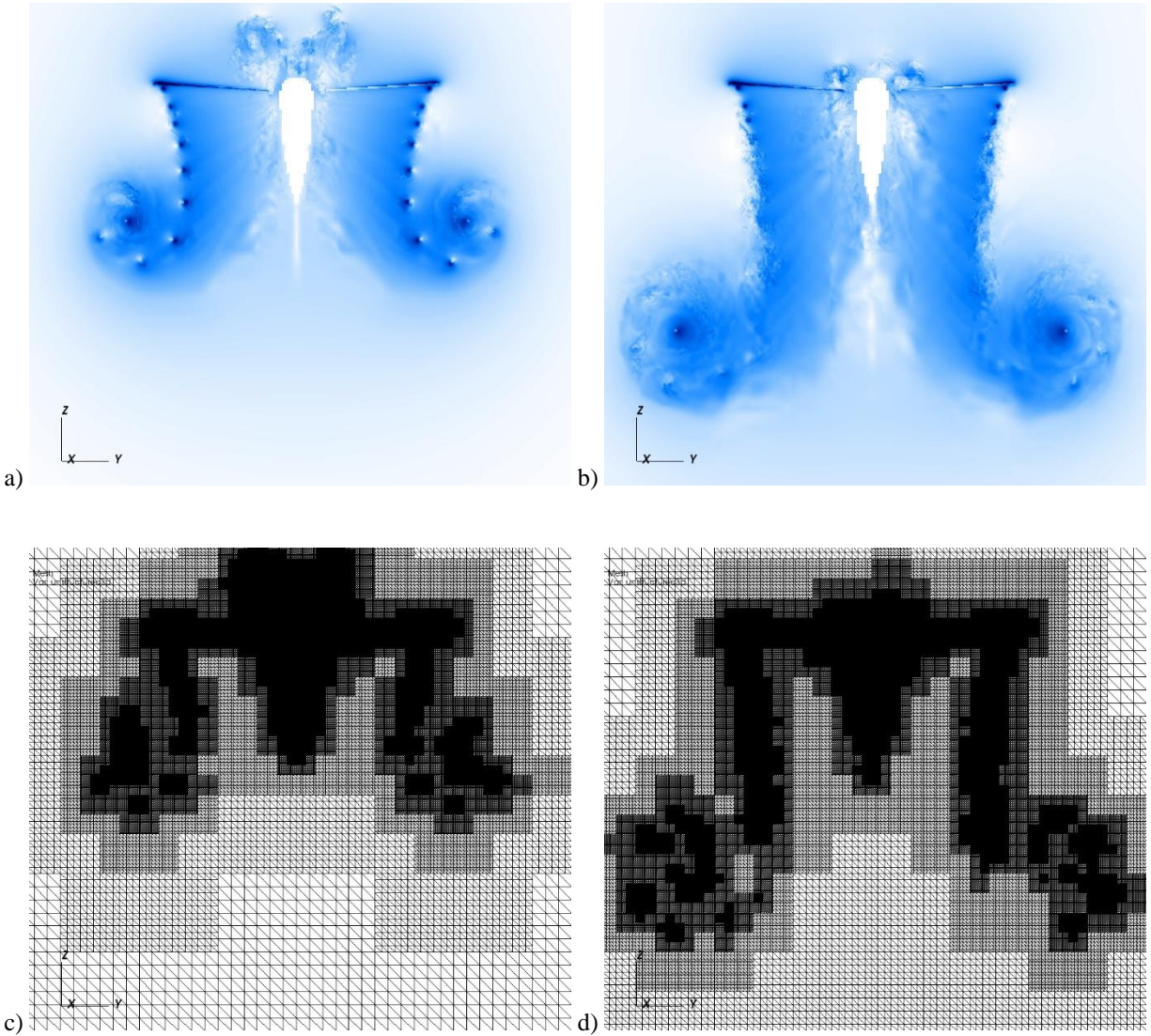
Figure 11. Wake dissipation over time for simulation with p_{max}=7. Velocity magnitude contours a) 5th revolution, b) 8th revolution. Mesh at c) 5th revolution, d) 8th revolution.
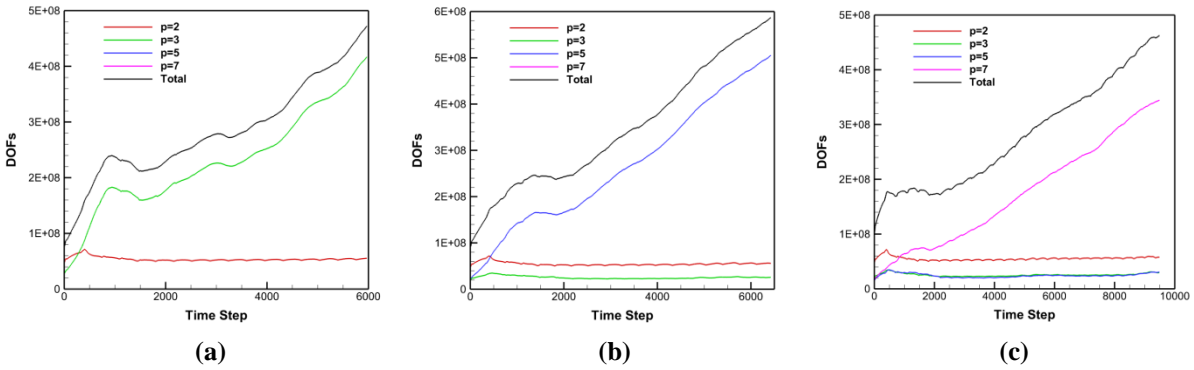
Figure 12. Number of degrees of freedom for the S-76 rotor simulation. a) Off-body mesh adaptation of $p_{max}=3$, 4th order of accuracy in the wake region. b) Off-body mesh adaptation of $p_{max}=5$, 6th order of accuracy in the wake region. c) Off-body mesh adaptation of $p_{max}=7$, 8th order of accuracy in the wake region.
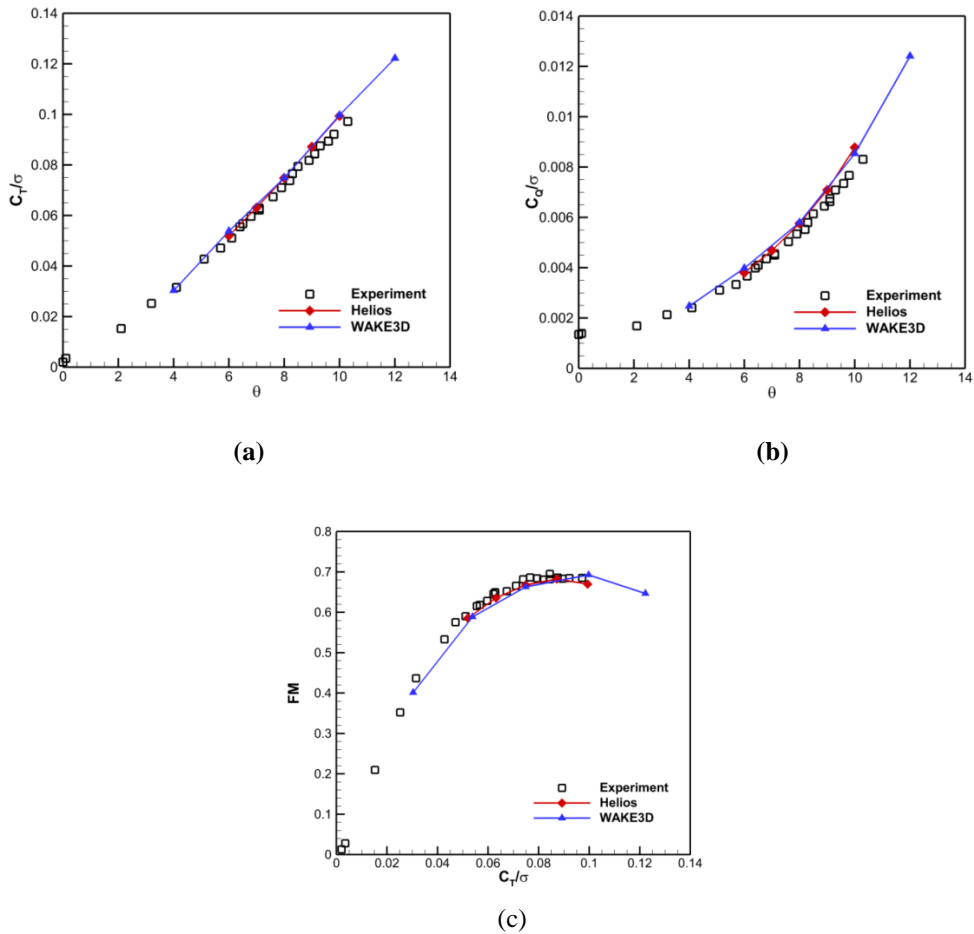

Figure 13. Simulation results of the S-76 rotor blade with the swept-tapered tip at $M_{tip}=0.65$. The W^2A^2KE3D results are compared to the experimental measurements[4] along with another numerical simulation: CREATE-AV HELIOS[24]. a) thrust coefficient, b) torque coefficient, and c) the figure of merit.